Results from the first all-sky search for continuous gravitational waves from small-ellipticity sources

Vladimir Dergachev[1, 2, a] and Maria Alessandra Papa[1, 2, 3, b]

[1]*Max Planck Institute for Gravitational Physics (Albert Einstein Institute), Callinstrasse 38, 30167 Hannover, Germany*
[2]*Leibniz Universität Hannover, D-30167 Hannover, Germany*
[3]*University of Wisconsin Milwaukee, 3135 N Maryland Ave, Milwaukee, WI 53211, USA*

We present the results of an all-sky search for continuous gravitational wave signals with frequencies in the 500-1700 Hz range targeting neutron stars with ellipticity of 10^{-8}. The search is done on LIGO O2 data set using Falcon analysis pipeline. The results presented here double the sensitivity over LIGO O2 data results [12, 29]. The search is capable of detecting low ellipticity sources up to 170 pc. We establish strict upper limits which hold for worst-case signal parameters. We list outliers uncovered by the search, including several which we cannot associate with any known instrumental cause.

Introduction Continuous gravitational waves are expected over a broad range of frequencies from rapidly rotating compact stars such as neutron stars due to a variety of mechanisms [1], as well as from more exotic scenarios [2–7].

A spinning neutron star that presents a deviation from axi-symmetry emits continuous gravitational waves. Its gravitational-wave brightness is determined by its equatorial ellipticity, which describes how deformed the star is in the plane perpendicular to the rotation axis. Because neutron stars have solar sized mass packed within a tight radius of 10-15 km, the gravity at their surface is extremely high, making it difficult to support large deformations.

Simulations show that ellipticities as high as 10^{-6} can be supported by the crust [8, 9], but at present no mechanism is known that mandates the existence of such deformations. Searches so far have failed to find signals from high ellipticity sources [10–14].

On the other hand, properties of observed pulsars suggest that a population might exist whose spin evolution is governed by gravitational wave emission, with typical ellipticities in the range of $\approx 10^{-9}$ to 10^{-8} [15]. This is the range targeted by this search (Figure 1).

We find several outliers and investigate them. We use longer coherence analyses and out-of-sample data. One outlier increases in SNR with increase in coherence length, however, this increase is not as large as one would expect for an ideal signal on average.

The basic signal assumed at the gravitational wave detector is a nearly monochromatic signal from an isolated source (i.e. not in a binary), with Doppler modulations due to the relative motion between the source and the detector and amplitude modulations due to the relative orientation of the detector to the source. Optimal sensitivity is typically achieved with a large degree of phase coherence in the signal and for signals matching the assumed waveform model.

No past search has revealed any such signal, over a broad range of possible signal parameters. One reason could be that past searches were not sensitive enough and
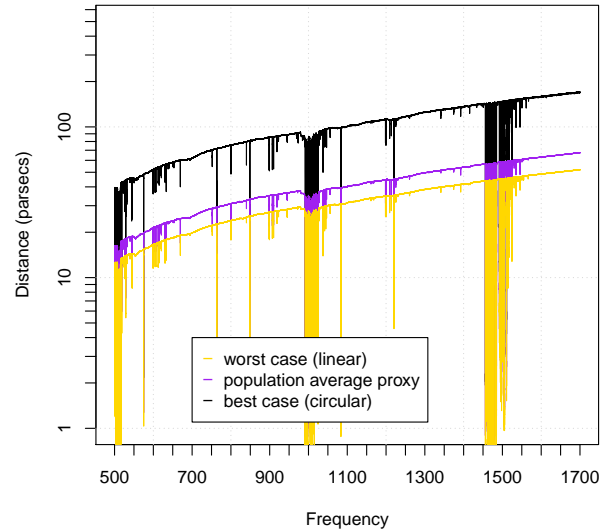

FIG. 1. Range of the search for stars with ellipticity of 10^{-8}.

have not yet probed low enough values of the ellipticity. Another reason (or perhaps an additional reason) might be that that the signals deviate enough from the assumed model that the search methods cannot identify them with sufficient confidence.

Deviations from the naive signal model could come about in a number of ways, for example due to the motion of the source being perturbed by another body, or the signal itself not being perfectly stable. While standard searches might retain very good sensitivity to many of these signals [16], upon closer inspection a signal candidate might be disregarded because it does not pass all the tests that the naive signal would pass.

As more and more sensitive searches yield null results it seems wise to entertain the possibility that the signals are not quite as we assume. In this paper we highlight the upper limit results for the standard signals, as well as the

top outliers that are marginal/inconclusive candidates.

The method Broad-band all-sky searches for continuous gravitational waves are computationally challenging. The most sensitive surveys employ multi-stage semi-coherent searches that rely on clever search methods, computationally efficient algorithms and much computing power.

Loosely coherent methods [17–19] fall in the broad category of semi-coherent searches. These combine together results from coherent searches over shorter time-baselines that together cover the entire observing period. The most prominent difference among existing semi-coherent schemes lies in the way that they combine the coherent search results – see [13, 14, 20–22] and references therein for an overview and comparison of the different families of semi-coherent search methods.

Loosely coherent methods estimate power with bilinear functions of the Fourier transforms of overlapping segments of data [17] and are purposely constructed to have a broad overlap reduction function in parameter space. Due to the overlap of the segments and with the use of appropriate kernels it is possible to tune a loosely coherent search to approximate a coherent search with a time-baseline longer than that of the input Fourier transforms, to attain robustness to deviations of the waveform from the standard model and to optimize computing performance on specific hardware.

The newest loosely coherent implementation targeting longer coherent timescales, the Falcon search, represents a breakthrough in performance and sensitivity [13]. We have explored the LIGO O1-run data employing the Falcon search with a first-stage coherent length of 4 hours, and demonstrated its performance and computational efficiency [10, 13]. In this paper we push the envelope further, doubling the size of the input data, tripling the coherence length of the first stage, extending the frequency range by a factor of nearly three and searching high frequencies[1]. We attain a two-fold increase in strain sensitivity with respect to the best LIGO all-sky search on the same data.

The search We aim at detecting continuous gravitational wave signals with frequency between $500 - 1700 \, \mathrm{Hz}$ and first-order frequency derivative $|f_1| \leq 3 \times 10^{-12} \, \mathrm{Hz/s}$ for frequencies below $1000 \, \mathrm{Hz}$ and $\leq 2.5 \times 10^{-12} \, \mathrm{Hz/s}$ above $1000 \, \mathrm{Hz}$. This is a generous range: the largest known frequency drift among pulsars spinning faster than $250 \, \mathrm{Hz}$ is $-1.73 \times 10^{-13} \, \mathrm{Hz/s}$, for the pulsar J1824-2452A spinning at $327 \, \mathrm{Hz}$ (gravitational wave frequency $654 \, \mathrm{Hz}$) [23].

We use the public LIGO [24] O2 data [25, 26]. Below 1000 Hz this data was subject to a cleaning procedure

---

[1] The necessary computing power scales as the cube of highest frequency searched

that removed a substantial amount of spurious instrumental noise [27]. In general this procedure will contribute an additional systematic uncertainty to the calibration, which is however not stated. We use the available O2 data as is, thus our results below 1000 Hz have a potential systematic uncertainty that overall should match the uncertainty (5% and 10% for H1 and L1 respectively) given in LIGO papers such as [12].

The search begins with a coherence length of 12 hours that is extended to 6 days through 3 follow-up stages (Table I). The coherence time-baseline increases from stage to stage and hence the sensitivity to a signal increases. Candidates pass to the next stage only if their detection statistic value exceeds a predetermined threshold value, which increases from one stage to the next. The last stage also includes consistency checks between the single-instrument results. Candidates that survive this entire sequence of tests represent one of the results of the search. We refer to these as the *outliers* from the search. Every outlier is defined by a set of signal parameters (frequency, sky position and frequency derivative) and signal to noise ratio value (SNR).
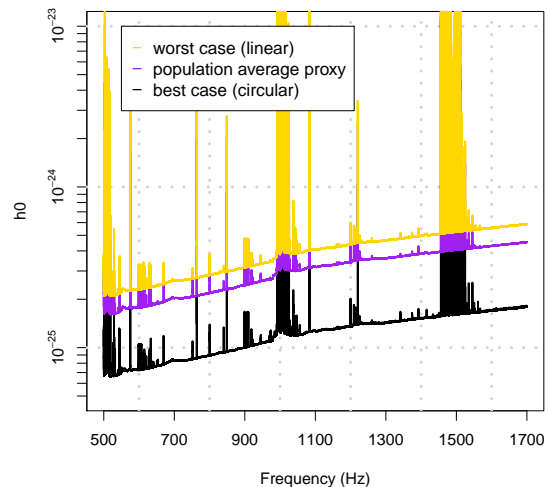

FIG. 2. The intrinsic gravitational-wave strain-amplitude upper-limit (vertical axis) is plotted against signal frequency. The upper (yellow) curve shows worst-case upper limits, the next lower curve (purple) shows the population-average proxy, followed by the black curve showing best-case upper limits (circularly polarized signals). The worst-case and best-case upper limits are maximized over sky and all intrinsic signal parameters for each frequency band displayed.

Upper limit results One of the results of the search are the 95% confidence-level continuous gravitational wave amplitude upper limits h_0. These represent the smallest amplitude of a continuous signal at a given frequency, with first and second order frequency drift in

Stage	Coherence length (hours)	Minimum SNR
0	12	6
1	24	7
2	48	8
3	144	16

TABLE I. Parameters for each stage of the search. The stage 3 outliers are subject to an additional consistency check.

Band [Hz]	$|f_1|_{max}$ 10^{-12} [Hz/s]	$|f_2|_{max}$ 10^{-20} [Hz/s^2]
500-1000	3	4
1000-1700	2.5	2

TABLE II. Signal-parameter space covered in this search. Both positive and negative values of frequency derivatives f_1 and f_2 are explored.

covered range (Table II) and coming from an arbitrary direction, that we can exclude from impinging on the detectors. We have assumed a quasi-monochromatic signal with slow evolution in frequency that can be approximated by a quadratic model:

$$f(t) = f_0 + (t - t_0)f_1 + (t - t_0)^2 f_2/2, \qquad (1)$$

where f_0 is the signal frequency at GPS epoch $t_0 = 1183375935$, and, as already defined, f_1 and f_2 are the linear and quadratic frequency drifts, respectively.

Our upper limits are established based on the observed power estimates and are valid even in the most heavily contaminated spectral regions [28] and, by construction, also in the presence of a signal.

We compute three upper-limits: the so-called worst-case upper limit which is the largest upper limit over those established for individual sky locations, polarization[2], spindown and frequency; the circular-polarization upper limit which is the largest upper limit over those established for individual sky locations, spindown and frequency, having assumed circular polarization of the signal; and finally a proxy for the population-average upper limit which is determined over a population of sources uniformly distributed on the sky and with all possible polarizations (uniform in the cosine of the inclination angle ($\cos \iota$) and polarization angle ψ). This last upper limit is provided for ease of comparison with other search results [11, 14, 29, 30] and it is estimated (hence it is a proxy) as a weighted average of the upper limits from the individual polarizations.

The population average proxy is verified by directly measuring the detection efficiency of fake signals added

---

[2] maximum over polarization is usually reached for linear polarizations

to the real data with frequencies in the 500-600 Hz band and in the 1075.40-1100 Hz band. These frequency regions are picked to reduce the computation cost of this procedure while still covering a large frequency range. Each fake signal has an intrinsic strain amplitude h_0 equal to the population-average upper-limit proxy value from its frequency band; other parameters are uniformly distributed in the searched parameter space, apart for the spindown values that are log-uniformly distributed in the search range. The full analysis is performed for each fake signal, covering the entire sky and including outlier follow-up. A fake signal is considered detected when an outlier is found within 5×10^{-5} Hz of the signal frequency f, within 10^{-12} Hz/s of its spindown, and within 0.06 Hz/f radians from its sky location location, the latter calculated after projection on the ecliptic plane ("ecliptic distance").
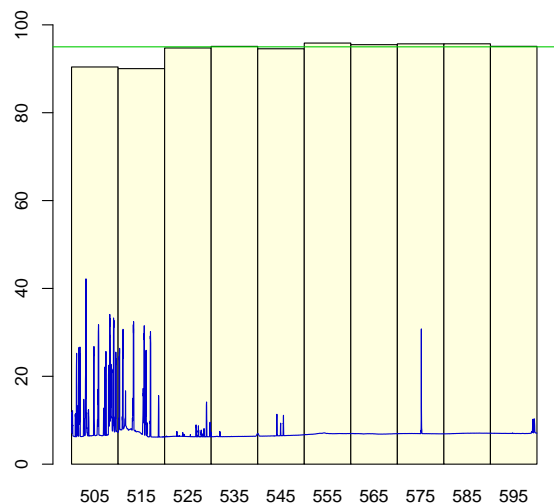

FIG. 3. The yellow bars show the detection efficiency of signals with amplitude at the population average (proxy) upper limit level, measured in 10 Hz bands. In each band we consider $\gtrsim 530$ fake signals. The top (green) line marks the 95% level. The blue curve on the bottom shows population average upper limits. We see that even in the heavily contaminated bands the detection efficiency is never lower than 90%.

We obtain 95% recovery of injections (Figure 3) everywhere except the heavily contaminated violin mode region, and even in those bands the detection efficiency does not drop lower than 90%.

The upper limits are plotted in Figure 2. The upper limit data is available in computer-readable format at [31].

Assuming an optimally oriented source of ellipticity 10^{-8} we are sensitive as far as 170 pc at 1700 Hz. Figure 1 shows detectable distance to such sources. Above 700 Hz

and excluding a few contaminated frequency bands, we can exclude the presence of such sources within a 20 pc distance from Earth. We expect the closest neutron star to be within this radius.

Our upper limits are relevant for boson condensates around black holes [3, 4], which are expected to emit monochromatic continuous wave signals [32]. Indeed, if ultralight bosons exist, they will form clouds around rotating black holes via superradiance instability and through annihilations and level transitions will emit continuous gravitational waves. We leave it to the interested reader to constrain from our upper limits physical quantities of interest, based on the specific model they wish to consider. Assuming the ensemble signal of [33] from a galactic population of $O(10^8)$ isolated stellar mass black holes with maximum mass 30 $M_\odot$ and maximum initial spin uniformly distributed in [0,1], our results exclude bosons with masses in the range $\approx [1.0-3.0] \times 10^{-12}$ eV.
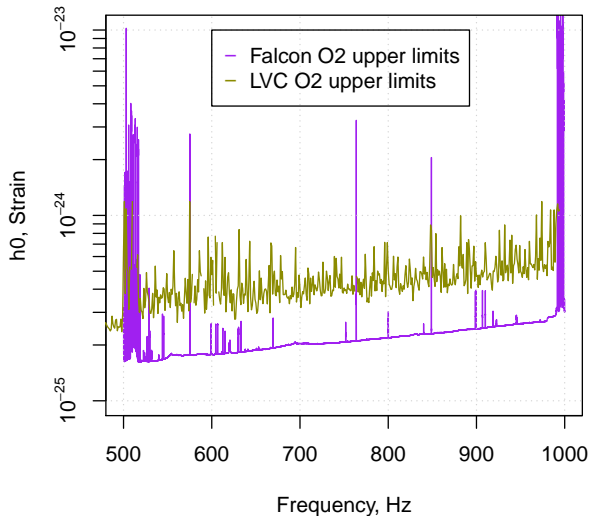

FIG. 4. Comparison of the Falcon O2 population-average upper limits (lower curve with tall spikes) and the LIGO-Virgo collaboration results [12] (upper curve). The dimensionless strain (vertical axis) is plotted against signal frequency.

Outliers The full list of outliers is available in [31]. Table III shows a summary of this list produced by displaying the largest SNR outlier in every 0.1 Hz band. This is especially helpful for the loud fake signals present in the data stream for validation purposes [34], since these produce many outliers. Because these fake signals are produced directly at the LIGO detectors by an appropriate excitation of its mirrors, they are commonly referred to as "hardware injections". In Table IV for convenience we give the parameters of these fake signals.

Our top 8 outliers in table III are caused by such

hardware-injections. The large majority of the remaining outliers are due to large hardware artifacts, as indicated in the last column of III. There remain outliers whose origin could perhaps be identified based on data from physical and environmental monitoring channels. Since this data is not public we cannot perform such investigations.

A key question is whether any of the listed outliers are produced by an astrophysical source. The simulations performed to verify the population average proxy assure us that if a signal were present in the data with detectable strength, there would be a corresponding outlier in table III. Clearly none of the outliers due to hardware injections are astrophysical. A number of outliers are not due to hardware injected signals but are located in frequency bands with instrumental contamination. As the pipeline is perfectly able to detect signals in most heavily contaminated bands this does not rule out these outliers. However, it does cast doubt on their significance as contamination can artificially increase the SNR in a single or both instruments.
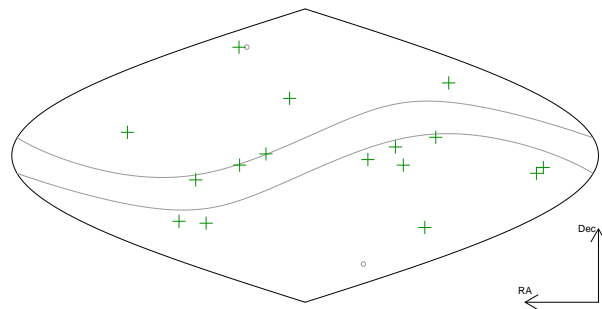

FIG. 5. Location in the sky of the outliers not associated to any instrumental disturbance. The wide band shows ecliptic plane, the two small circles are the ecliptic poles.

The 16 outliers not associated with any known instrumental disturbance are the most interesting. Their sky locations are shown in figure 5. They do not appear to cluster in any location (such as the ecliptic pole) tied to instrumental artifacts. If the outliers were due to astrophysical signals that follow the frequency model of Eq. 1, then the uncertainty on their true location would be within the limits established by the Monte Carlo simulations discussed above, i.e. $0.06 \, \text{Hz}/f$ radians, projected on the ecliptic plane.

The frequency spectrum of these outliers is manually examined and none reveals any obvious contamination. As an example we show plots (Figures 6 and 7) corresponding to highest-frequency outlier 43 at 1224.75 Hz. The apparent frequency of a signal with the parameters of outlier 43, spans almost 0.25 Hz during the O2 observing time and its evolution is shown in Figure 6.

The other 15 outliers have similar characteristics. The frequency evolution curves change depending on the out-
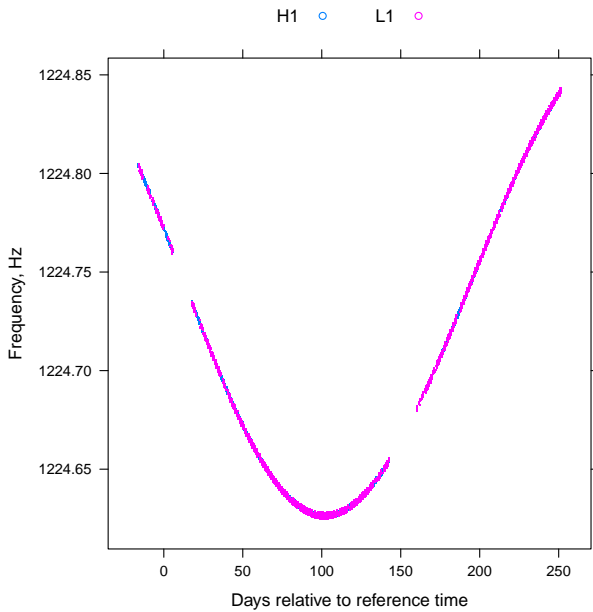
FIG. 6. Apparent frequency of a signal with parameters equal to those of outlier 43 at 1224.74 Hz, at the detectors. The difference in Doppler shifts between interferometers is small compared to the Doppler shifts from the Earth's orbital motion.
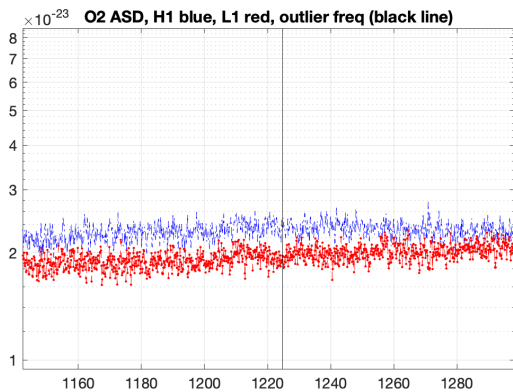

FIG. 7. Average amplitude spectral density around the frequency of outlier 43.

lier parameters but they all exhibit an appreciable modulation.

Ad-hoc investigations are focused on outliers 25 and 43, which are consistently found with both the Falcon and the semi-coherent F-statistic analyses. Follow-ups over longer coherence lengths (up to 500 hours) suggest that the most promising outlier is outlier 25. We note that the f_1 value of outlier 25 is positive which would mean that, if the outlier were associated to an astrophysical continuous signal, what is observed is *not* directly related to the spin frequency of the star.

The SNR build-up for outlier 25 over searches with in-

creasingly long coherent time baseline is not inconsistent with what is expected from a signal. This holds true also for the fully coherent search over the O2 data, albeit the recovered SNR is lower than the expectation value based on the previous stages and with indications that the coherence might not be completely stable [3]. A follow-up on O1 data is inconclusive: the detection statistic value is not inconsistent with the expectations under the signal hypothesis, and the Gaussian-noise p-value is $\lesssim 1\%$.

As already pointed out, we are unable to investigate the O1 and O2 instrumental data channels, as this data is not part of either the O1 or O2 public data releases.

The best confirmation of the astrophysical origin of an outlier is to find a counterpart with independent data, be it new gravitational wave data, or radio, X-ray, gamma or from particle detector observations.

Our outliers are not present in the outlier lists from earlier papers. This is not surprising, because previous searches on LIGO O2 data that cover the parameter space of this search [12, 29] are about a factor of 2 less sensitive.

The O3 data is roughly a factor of 2 more sensitive than the O2 data employed in this search so the LIGO/Virgo broad-band searches should be able to probe continuous gravitational wave amplitudes comparable to these. Also, targeted searches based on the information presented here, which are comparatively less complex than these broad surveys, should be straightforward. We look forward to comparing our results on O3 data with those from the LVC, and we are ready to perform fast-turnaround investigations on new data.

---

[3] The most significant measured $2\mathcal{F}$ value is ≈ 47. $2\mathcal{F}$ is the optimal multi-detector fully coherent detection statistic [35] for signals of the type of Eq. 1.

Idx	SNR	Frequency Hz	Spindown pHz/s	RA$_{J2000}$ degrees	DEC$_{J2000}$ degrees	Description
1	15792.0	763.84732	−0.20	198.894	75.690	Injected pulsar ip9
2	11970.1	575.16352	−0.20	215.256	3.445	Injected pulsar ip2
3	2470.1	848.95675	−0.80	38.563	−30.432	Induced by injected pulsar ip1
4	88.7	1220.55117	0.00	218.862	24.074	Injected pulsar ip7
5	64.1	575.20332	−1.80	184.911	38.083	Induced by injected pulsar ip2
6	38.1	849.00348	2.60	67.737	−11.166	Induced by injected pulsar ip1
7	36.3	848.89699	1.00	353.084	−56.879	Induced by injected pulsar ip1
8	26.4	763.77799	−2.20	222.633	−68.689	Induced by injected pulsar ip9
9	22.3	1004.27599	−1.08	294.094	−88.258	Disturbed H1 spectrum, lines in L1
10	19.8	986.28829	−3.20	21.424	75.556	Coincident lines in H1 and L1
11	19.4	1006.24309	1.08	97.733	−67.657	Disturbed H1 spectrum, lines in L1
12	18.4	575.09518	−2.00	296.704	30.014	Induced by injected pulsar ip2
13	18.2	990.50363	−3.60	318.140	61.085	Line in L1
14	18.1	1392.54524	−0.70	236.558	43.756	Induced by injected pulsar ip4
15	17.7	900.21880	−2.20	119.428	−5.859	
16	17.6	1021.84249	−0.70	13.986	−8.813	Sharp line in L1
17	17.6	968.58972	−1.80	338.891	−76.549	Line in H1
18	17.4	1392.47501	−0.72	215.544	−33.472	Induced by injected pulsar ip4
19	17.4	514.14893	1.60	124.356	5.300	
20	16.9	1220.62294	1.44	256.566	65.131	Induced by injected pulsar ip7
21	16.8	997.54586	−1.80	210.349	46.174	Disturbed H1 spectrum
22	16.8	995.20385	1.40	205.113	48.184	Disturbed H1 spectrum
23	16.7	1001.36623	4.30	77.684	−44.133	
24	16.6	676.19542	2.80	220.418	−5.822	
25	16.6	744.21917	2.40	191.654	35.097	
26	16.5	998.97311	−2.00	51.221	11.566	Disturbed H1 spectrum, line in L1
27	16.4	997.41470	1.40	345.963	−27.957	Disturbed H1 spectrum
28	16.4	991.29230	2.20	48.300	−60.960	Disturbed H1 spectrum
29	16.4	512.49081	1.20	141.462	−2.467	
30	16.3	991.10725	0.40	313.415	61.938	Disturbed H1 spectrum, line in L1
31	16.3	983.15189	2.20	204.037	1.030	
32	16.3	988.60680	1.80	145.053	−44.240	Lines in H1 and L1
33	16.3	510.79524	−2.40	23.196	−5.131	Disturbed L1 spectrum
34	16.2	886.88009	−1.60	281.482	−40.307	
35	16.2	988.37320	1.20	56.255	44.595	
36	16.2	512.26233	3.00	334.102	−12.737	Line in L1
37	16.2	963.34281	−2.80	306.751	59.163	Line in H1
38	16.2	1580.37607	−2.50	11.198	32.482	Line in L1
39	16.1	514.29168	3.20	32.603	−7.354	
40	16.1	831.98847	0.40	281.743	66.494	
41	16.1	873.52461	0.40	35.466	−10.855	
42	16.1	895.42195	3.60	292.529	14.276	
43	16.0	1224.74567	−2.16	98.278	11.241	
44	16.0	1014.34897	−2.50	25.330	82.271	Lines in H1 and L1
45	16.0	698.72803	−0.20	261.117	−41.490	
46	16.0	1095.55740	−1.08	249.504	−14.911	

TABLE III. Outliers produced by the detection pipeline. Only the highest-SNR outlier is shown for each 0.1 Hz frequency region. Outliers marked with "line" have strong narrowband disturbances near the outlier location. Signal frequencies refer to epoch GPS 1183375935.

[a] vladimir.dergachev@aei.mpg.de
[b] maria.alessandra.papa@aei.mpg.de

[1] P. D. Lasky, Gravitational Waves from Neutron Stars: A Review, Publ. Astron. Soc. Austral. **32**, e034 (2015)
[2] R. Brito, S. Ghosh, E. Barausse, E. Berti, V. Cardoso, I. Dvorkin, A. Klein and P. Pani, Gravitational wave searches for ultralight bosons with LIGO and LISA, Phys. Rev. D **96**, no. 6, 064050 (2017)
[3] M. Baryakhtar, R. Lasenby, M. Teo, Black Hole Superradiance Signatures of Ultralight Vectors, Phys. Rev. D **96**, 035006s (2017)
[4] A. Arvanitaki, M. Baryakhtar, R. Lasenby, S. Dimopoulos, S. Dubovsky, Black Hole Mergers and the QCD Axion at Advanced LIGO, Phys. Rev. D **95**, 043001 (2017)

Label	Frequency Hz	Spindown pHz/s	RA$_{J2000}$ degrees	DEC$_{J2000}$ degrees
ip1	848.969641	300	37.39385	−29.45246
ip2	575.163521	-0.137	215.25617	3.44399
ip4	1393.540559	-254	279.98768	−12.4666
ip7	1220.555270	-1120	223.42562	−20.45063
ip9	763.847316	-1.45×10^{-5}	198.88558	75.68959

TABLE IV. Parameters of the hardware-injected simulated continuous wave signals during the O2 data run (epoch GPS 1130529362).

[5] A. Arvanitaki, M. Baryakhtar, X. Huang, Discovering the QCD Axion with Black Holes and Gravitational Waves, Phys. Rev. D **91**, 084011 (2015)

[6] C. J. Horowitz and S. Reddy, Gravitational Waves from Compact Dark Objects in Neutron Stars, Phys. Rev. Lett. **122**, no. 7, 071102 (2019)

[7] C. J. Horowitz, M. A. Papa and S. Reddy, Gravitational waves from compact dark matter objects in the solar system, arXiv:1902.08273

[8] C. J. Horowitz and K. Kadau, Breaking Strain of Neutron Star Crust and Gravitational Waves, Phys. Rev. Lett. **102**, 191102 (2009).

[9] N. K. Johnson-McDaniel and B. J. Owen, Maximum elastic deformations of relativistic stars, Phys. Rev. D **88**, 044004 (2013)

[10] V. Dergachev and M. A. Papa, Results from an extended Falcon all-sky survey for continuous gravitational waves, Phys. Rev. D **101**, 022001 (2020)

[11] B. P. Abbott *et al.* (LIGO Scientific Collaboration and Virgo Collaboration), Full Band All-sky Search for Periodic Gravitational Waves in the O1 LIGO Data, Phys. Rev. D **97** 102003 (2018).

[12] B. P. Abbott *et al.* (LIGO Scientific Collaboration and Virgo Collaboration), All-sky search for continuous gravitational waves from isolated neutron stars using Advanced LIGO O2 data, Phys. Rev. D **100** 024004 (2019).

[13] V. Dergachev and M. A. Papa, Sensitivity Improvements in the Search for Periodic Gravitational Waves Using O1 LIGO Data, Phys. Rev. Lett. **123**, no. 10, 101101 (2019)

[14] B. P. Abbott *et al.* (LIGO Scientific and Virgo Collaborations), First low-frequency Einstein@Home all-sky search for continuous gravitational waves in Advanced LIGO data, Phys. Rev. D **96**, no. 12, 122004 (2017)

[15] G. Woan, M. D. Pitkin, B. Haskell, D. I. Jones, and P. D. Lasky, Evidence for a Minimum Ellipticity in Millisecond Pulsars, ApJL **863** L40 (2018)

[16] A. Singh, M. A. Papa and V. Dergachev, Characterizing the sensitivity of isolated continuous gravitational wave searches to binary orbits, Phys. Rev. D **100** (2019) no.2, 024058 doi:10.1103/PhysRevD.100.024058

[17] V. Dergachev, On blind searches for noise dominated signals: a loosely coherent approach, Class. Quantum Grav. **27**, 205017 (2010).

[18] V. Dergachev, Loosely coherent searches for sets of well-modeled signals, Phys. Rev. D **85**, 062003 (2012)

[19] V. Dergachev, Loosely coherent searches for medium scale coherence lengths, Phys. Rev. D **85**, 062003 (2012)

[20] S. Walsh, K. Wette, M. A. Papa and R. Prix, Optimizing the choice of analysis method for all-sky searches for continuous gravitational waves with Einstein@Home, Phys. Rev. D **99**, no. 8, 082004 (2019)

[21] S. Walsh *et al.*, Comparison of methods for the detection of gravitational waves from unknown neutron stars, Phys. Rev. D **94**, no. 12, 124010 (2016)

[22] C. Dreissigacker, R. Prix, K. Wette, Fast and Accurate Sensitivity Estimation for Continuous-Gravitational-Wave Searches, Phys. Rev. D **98**, 084058 (2018)

[23] R.N. Manchester, G.B. Hobbs, A. Teoh, M. Hobbs, AJ, 129, 1993-2006 (2005)

[24] J. Aasi *et al.* (LIGO Scientific Collaboration), Advanced LIGO, Class. Quantum Grav. **32** 7 (2015)

[25] M. Vallisneri *et al.* The LIGO Open Science Center, proceedings of the 10th LISA Symposium, University of Florida, Gainesville, 2015 J. Phys.: Conf. Ser. 610 012021

[26] LIGO Open Science Center, `https://doi.org/10.7935/CA75-FM95`, (2019)

[27] J.C. Driggers *et al.* (LIGO Scientific Collaboration Instrument Science Authors), Improving astrophysical parameter estimation via offline noise substraction for Advanced LIGO, Phys. Rev. D **99**, 042001 (2019).

[28] V. Dergachev, A Novel Universal Statistic for Computing Upper Limits in Ill-behaved Background, Phys. Rev. D **87**, 062001 (2013).

[29] C. Palomba *et al.*, Direct constraints on ultra-light boson mass from searches for continuous gravitational waves, Phys. Rev. Lett. **123**, 171101 (2019)

[30] B. P. Abbott *et al.* (LIGO Scientific Collaboration and Virgo Collaboration), All-sky Search for Periodic Gravitational Waves in the O1 LIGO Data, Phys. Rev. D **96**, 062002 (2017)

[31] See EPAPS Document No. [number will be inserted by publisher] for numerical values of upper limits. Also at `https://www.aei.mpg.de/continuouswaves/O2Falcon500-1700`

[32] A. Arvanitaki, M. Baryakhtar, and X. Huang, Discovering the QCD axion with black holes and gravitational waves, Phys. Rev. D **91**, 084011 (2015)

[33] S. J. Zhu, M. Baryakhtar, M. A. Papa, D. Tsuna, N. Kawanaka and H. Eggenstein, Characterizing the continuous gravitational-wave signal from boson clouds around Galactic isolated black holes, [arXiv:2003.03359 [gr-qc]].

[34] O2 continuous hardware injection signal parameters `https://www.gw-openscience.org/O2_injection_params`

[35] C. Cutler and B. F. Schutz, The Generalized F-statistic: Multiple detectors and multiple GW pulsars, Phys. Rev. D **72** (2005), 063006